

An Orientation Selective Neural Network and its Application to Cosmic Muon Identification

Halina Abramowicz

Deutsches Elektronen-Synchrotron DESY, Hamburg

and

School of Physics and Astronomy, Tel Aviv University

David Horn, Ury Naftaly, Carmit Sahar–Pikielny

School of Physics and Astronomy, Tel Aviv University

Tel Aviv 69978, Israel

Abstract

We propose a novel method for identification of a linear pattern of pixels on a two-dimensional grid. Following principles employed by the visual cortex, we employ orientation selective neurons in a neural network which performs this task. The method is then applied to a sample of data collected with the ZEUS detector at HERA in order to identify cosmic muons which leave a linear pattern of signals in the segmented uranium-scintillator calorimeter. A two dimensional representation of the relevant part of the detector is used. The results compared with a visual scan point to a very satisfactory cosmic muon identification. The algorithm performs well in the presence of noise and pixels with limited efficiency. Given its architecture, this system becomes a good candidate for fast pattern recognition in parallel processing devices.

1 Introduction

A typical problem of experiments performed at high energy accelerators aimed at studying novel effects in the field of Elementary Particle Physics is the need to preselect interesting interactions at as early a stage as possible, in order to keep the data volume manageable. One class of events which have to be eliminated is due to cosmic muons which pass all trigger conditions.

The most characteristic feature of cosmic muons is that they leave in the detector a path of signals aligned along a straight line. The efficiency of pattern recognition algorithms depends strongly on the granularity with which such a line is probed, on the level of noise and the response efficiency of a given detector. Yet the efficiency of a visual scan is fairly independent of those features. This lead us to look for a new approach through application of ideas from the field of vision.

The visual cortex performs the difficult task of constructing the image of the 3D external reality [1, 2] from the signals which are based on 2D retinal images. Our problem is clearly different, yet it has some similarities. The information gathered in a detector has finite and different resolution in different locations, can be multivariate in nature (e.g. location and energy deposition), and has empty regions where no signals come from. Often the vision problem is described as achieving a balanced integration of all different inputs to obtain the general content of the picture. Here we look for some characteristic detail in order to classify the event into some particular category. This calls for a differentiation of the information, neglecting sometimes most of the available data and retaining only some key features.

The main tool which we will borrow from the neuronal circuitry of the visual cortex is the orientation selective simple cell [3]. It will be incorporated in the hidden layers of a feed forward neural network, possessing a predefined receptive field with excitatory and inhibitory connections. Using these elements we develop a method for identifying straight lines of varying slope and length on a grid with limited resolution. This method is then applied to the problem of identifying cosmic muons in accelerator data, and compared with other tools.

2 Description of the Task

This work was motivated by the observation that a visual scan, albeit time consuming, is by far the most trustworthy and efficient way of identifying cosmic muon events, in this case in the analysis of electron proton interactions with the ZEUS detector [4] at HERA.

We try to employ a neural network (NN) which captures the key elements of the visual scan. We limit ourselves at this stage to cosmic muons which enter the rear part of the ZEUS calorimeter in the direction perpendicular to

the beam-line. Because of a catastrophic energy loss in the electromagnetic cells of the calorimeter they mimic an electron trigger, which is the basis for selecting deep inelastic electron proton interactions [5]. It should be noted however that these muons do not affect the physics analysis, their contamination is estimated to be well below 1%.

In a two-dimensional representation the granularity of the rear part of the ZEUS calorimeter [6] can be emulated roughly by a 23×23 lattice of 20×20 cm² squares. While such a representation does not use the full information available in the detector, it is sufficient for our study. In our language each cell of this lattice will be denoted as a pixel. A pixel is activated if the corresponding calorimeter cell is above a threshold level predetermined by the properties of the detector.

A cosmic muon, depending on its angle of incidence, activates along its linear path typically from 3 to 25 neighboring pixels anywhere on the 23×23 grid. The pattern of signals generated by accelerator events consists on average of 3 to 8 clusters, of typically 4 adjacent activated pixels, separated by empty pixels. The clusters tend to populate the center of the 23×23 lattice. Due to inherent dynamics of the interactions under study, the distribution of clusters is not isotropic. Examples of events, as seen in the two-dimensional projection in the rear part of the ZEUS calorimeter, are shown in figure 1.

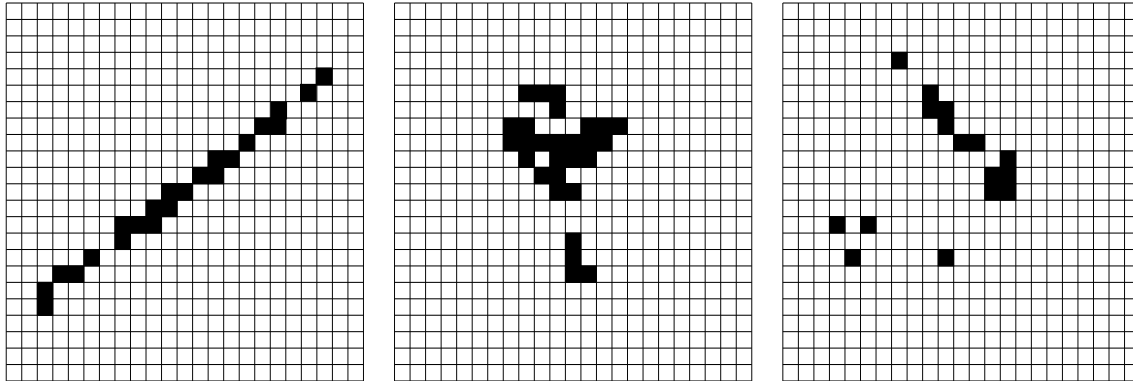


Figure 1: Example of patterns corresponding to a cosmic muon (left), a typical accelerator event (middle), and an accelerator event which looks like a muon (right), as seen in a two dimensional projection.

The lattice discretizes the data and distorts it. Adding conventional noise levels, the decision of classification of the data into accelerator events and cosmic muon events is difficult to obtain through automatic means. Yet, it is the conventional feeling of experimentalists dealing with these problems, that any expert can distinguish between the two cases with high efficiency (identifying a muon as such) and purity (not misidentifying an accelerator event). We define our task as developing automatic means of doing the same.

3 The Orientation Selective Neural Network

Our analysis will be based on a network of orientation selective neurons (OSNN) which will be described in this chapter. We start out with an input layer of pixels on a two dimensional grid with discrete labeling $i = (x, y)$ of the neuron (pixel) which can get the values $S_i = 1$ or 0 , depending on whether the pixel is activated or not.

The input is being fed into a second layer which is composed of orientation selective neurons $V_2^{i,\alpha}$ at location i with orientation θ_α where α belongs to a discrete set of 16 labels, i.e. $\theta_\alpha = \alpha\pi/16$. The neuron $V_2^{i,\alpha}$ is the analog of a simple cell in the visual cortex. The principle of its design is presented in Figure 2. Its receptive field consists of an array of dimension 5×5 centered at pixel i . The angle θ_α determines the orientation of a thin ellipse centered at i which encompasses an area of positive weights: each neuron, S_j , at the input layer whose pixel is intersected by this ellipse with a fractional geometrical overlap larger than $1/2$ excites $V_2^{i,\alpha}$ with weight $W_2^{i,\alpha,j} = 1$.

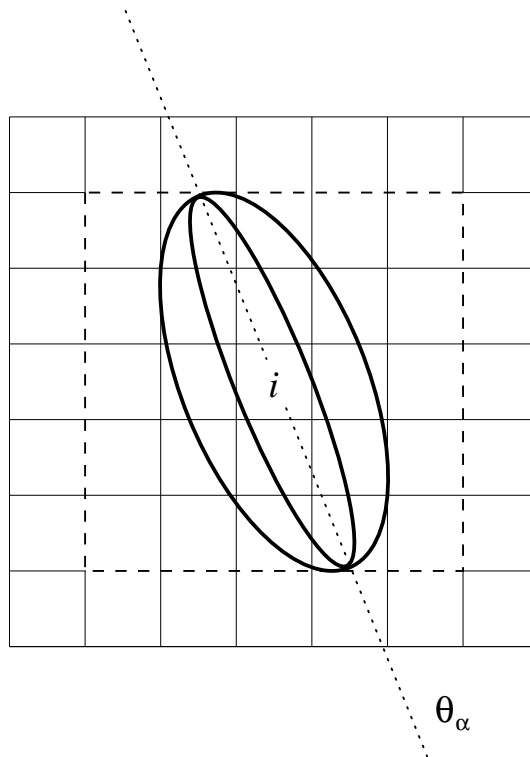


Figure 2: The receptive field of a $V_2^{i,\alpha}$ neuron centered around the pixel i with orientation $\theta_\alpha = 101.5^\circ$.

The value of the weights $W_2^{i,\alpha,j}$ can be 1, 0 and -1. The negative weights are attributed to the pixels which belong to the 5×5 subgrid but lie outside the fat ellipse, while the positive values were assigned inside the el-

lipse. All remaining weights are 0. Symbolically we may write the activation function of the neuron on the second layer as,

$$V_2^{i,\alpha} = \mathcal{F}_2\left(\sum_j W_2^{i,\alpha,j} S_j - T_2\right), \quad (1)$$

where T_2 is a threshold value, and $\mathcal{F}_2(x) = (x + T_2)\Theta(x)$. The values of $V_2^{i,\alpha}$ range from 0 to 5. The second layer consists then of $23 \times 23 \times 16$ neurons, each of which may be thought of as one of 16 orientation elements at some (x, y) location of the input layer. Next we employ a modified Winner Take All (WTA) algorithm, selecting the leading orientation $\alpha_{max}(i)$ for which the largest $V_2^{i,\alpha}$ is obtained at the given location i . If we find that several $V_2^{i,\alpha}$ at the same location i are close in value to the maximal one, we allow up to five different $V_2^{i,\alpha}$ neurons to remain active at this stage of the processing, provided they all lie within a sector of $\alpha_{max} \pm 2$, or $\theta_{max} \pm \pi/8$. All other $V_2^{i,\alpha}$ are reset to zero. If, however, at a given location i we obtain several large values of $V_2^{i,\alpha}$ which correspond to non-neighboring orientations, all are being discarded.

The third layer also consists of orientation selective cells. They are constructed with a receptive field of size 7×7 , and receive inputs from neurons with the same orientation on the second layer. The weights $W_3^{i,\alpha,j}$ are defined in a similar fashion to $W_2^{i,\alpha,j}$. The activation function of neurons of the third layer is

$$V_3^{i,\alpha} = \mathcal{F}_3\left(\sum_j W_3^{i,\alpha,j} V_2^{j,\alpha} - T_3\right), \quad (2)$$

where the index 3 stands for the quantities relevant to the third layer. The sum over j now runs over the larger receptive field. T_3 is the threshold value for the third layer and $\mathcal{F}_3(x) = (x + T_3)\Theta(x)$. For linear patterns, the purpose of this layer is to fill in the holes due to fluctuations in the pixel activation, i.e. complete the lines of same orientation of the second layer. As before, we keep also here up to five highest values at each location, following the same WTA procedure as on the second layer.

The fourth layer of the OSNN consists of only 16 components, D^α , each corresponding to one of the discrete orientations α . For each orientation we calculate two global sums which are convolutions of the first and third layers,

$$M^\alpha = \sum_i V_3^{i,\alpha} S_i \quad N^\alpha = \sum_i V_3^{i,\alpha} (1 - S_i). \quad (3)$$

The elements M^α carry the information about the number of the input pixels that contribute to a given orientation θ_α while N^α represent the mismatch between the neurons on the third layer and the corresponding input pixels.

An example of the OSNN procedure applied to an accelerator event is shown in Figure 3. The event is representative of a class of patterns which are

easily misidentified as cosmic muons. For the sake of simplicity we limit ourselves in this demonstration to only four orientations, $\theta_\alpha = 0^\circ, 45^\circ, 90^\circ, 135^\circ$, defined such that $\theta_\alpha = 0^\circ$ corresponds to the horizontal and $\theta_\alpha = 90^\circ$ to the vertical lines in the figure. The convolution of the third layer with the input (fourth layer) leads to the following results:

$$\begin{aligned}
 M_{0^\circ} &= 2 & N_{0^\circ} &= 1 \\
 M_{45^\circ} &= 0 & N_{45^\circ} &= 0 \\
 M_{90^\circ} &= 4 & N_{90^\circ} &= 3 \\
 M_{135^\circ} &= 5 & N_{135^\circ} &= 4
 \end{aligned}$$

The elements D^α defined as

$$D^\alpha = M^\alpha - N^\alpha, \quad (4)$$

will serve as the basis for performing our task. Cosmic muons are characterized by high values of D^α whereas accelerator events possess low values. The simplest decision method is to make a cut between the high and low values. A more sophisticated approach is to use a simple neural network to perform the analysis of the D^α . Both methods will be discussed in the next chapter.

To explain the reason for the choice of the fourth layer, we have to return to the origin of our analysis. Since the orientation selective elements act locally, and since accelerator events usually do not have an overall orientation, we expect the orientation selective neurons on the second and third layers to exhibit, for different angles, activity patterns which do not resemble the input pattern. On the other hand, cosmic muons should generate, for the appropriate orientation, activity patterns which resemble the input.

Because of the granularity and spatial resolution of our problem we have to allow on the second layer the possibility of several coexisting active neurons. This introduces a multiple working hypothesis into the next steps to which the final decision is deferred. In the final calculational step we assign a figure of merit which we want to maximize. This is built on the general intuition that the strongest signal for a consistent straight line in one orientation should be obtained from the orientation selective elements that lie on this line in the data. Subtracting the effect of orientation neurons which lie where no original pixels are excited, is needed in order to discard accelerator events where accidentally M^α may be large and yet the event is very different in shape from a single muon.

The complexity of this algorithm is $\mathcal{O}(n)$ where n is the number of pixels, since a constant number of operations is performed on each pixel. There are basically four free parameters in the algorithm. These are the size of the receptive fields on the second and third layer and the corresponding activation thresholds. Their values can be tuned for the best performance, however they are well constrained by the spatial resolution, the noise level

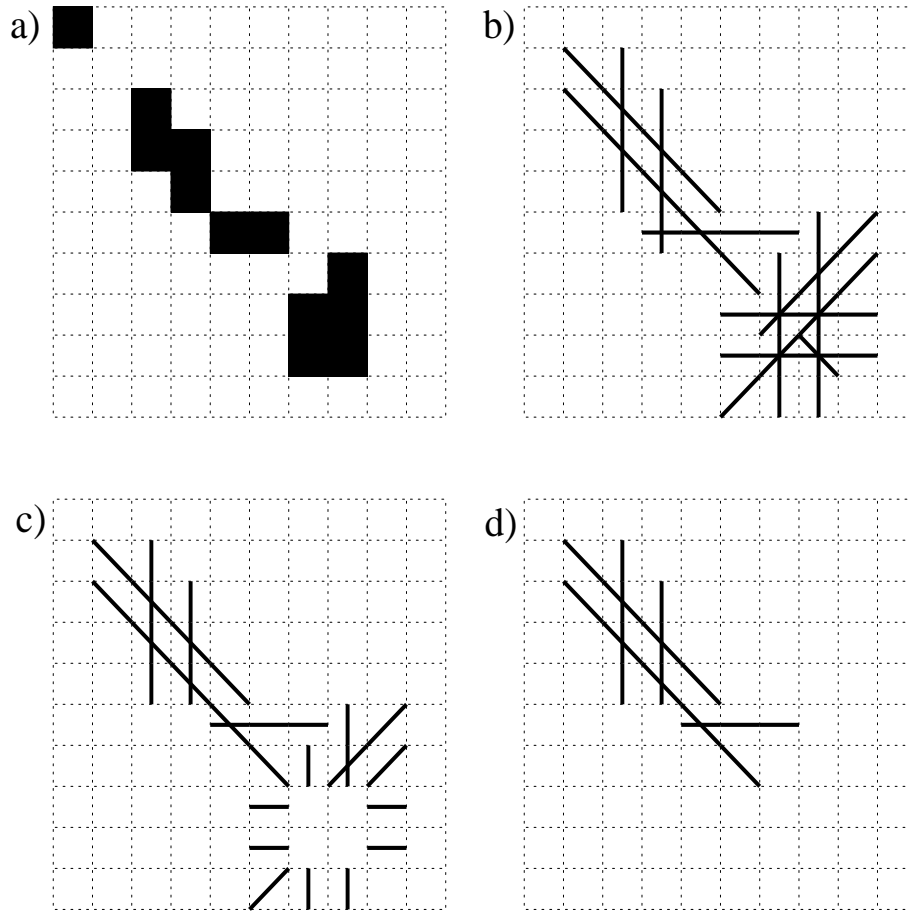


Figure 3: Demonstration of the OSNN filtering applied to the right most pattern presented in figure 1. a) A fragment of the lattice representing the input layer – each small square represents a pixel. b) Map of neurons which are activated in the second layer. Each small square represents a neuron whose orientation is designated by the line contained within the square. c) Map of neurons surviving on the second layer after application of the modified WTA algorithm. d) Neurons activated on the third layer.

in the system and the activation properties of the input pixels. The size of the receptive field determines to a large extent the number of orientations allowed to survive in the modified WTA algorithm.

4 Training of the OSNN

The details of the design of the OSNN and the tuning of its parameters were fixed while training it on a sample of 250 cosmic muons and a similar amount of accelerator events. The sample was obtained as a result of a preselection with existing algorithms and a visual scan as a cross-check.

The size of the receptive fields was described in the previous section. It is a compromise between a well defined orientation and the length of a cosmic muon for which the algorithm becomes applicable. The thresholds were chosen as $T_2 = 2.5$ and $T_3 = 4.5$.

For cosmic muon events the highest value of D^α determines the orientation of the straight line, θ_{OSNN} . This angle can be compared to the angle θ_{fit} , obtained from a conventional straight line fit. The results are shown in figure 4 where we plot the difference $\theta_{\text{fit}} - \theta_{\text{OSNN}}$ as a function of the number n_p of input pixels. We observe a good correlation between the two angles. The spread in $\theta_{\text{fit}} - \theta_{\text{OSNN}}$ reflects the spatial resolution of the lattice and justifies the use of the modified WTA with an angular uncertainty of $\pm\pi/8$. The small contribution of erroneous results observed for very low values of n_p is not surprising in view of the sizes of our ellipses.

In figure 5 we present the correlation between the maximum value of D^α , D_{max} , and the number n_p of input pixels for cosmic muon and accelerator events. As expected one observes a linear correlation between D_{max} and n_p for the muons while almost no correlation is observed for accelerator events. Above $D_{\text{max}} = 5$ there is a very clear separation between cosmic muon and accelerator events. This will define our first separation procedure which will be called OSNN- D .

We will quantify the quality of the selection by quoting the efficiency of properly identifying a cosmic muon for 100% purity, corresponding to no accelerator event misidentified as a muon. In the OSNN- D , where we require for a cosmic muon $D_{\text{max}} \geq 5$, we achieve 92.2% efficiency.

A better separation can be achieved with more sophisticated selection criteria which use more information from the fourth layer. Alternative methods will be discussed below. Clearly such procedures will be affected by the type of backgrounds to the linear patterns that one wants to isolate.

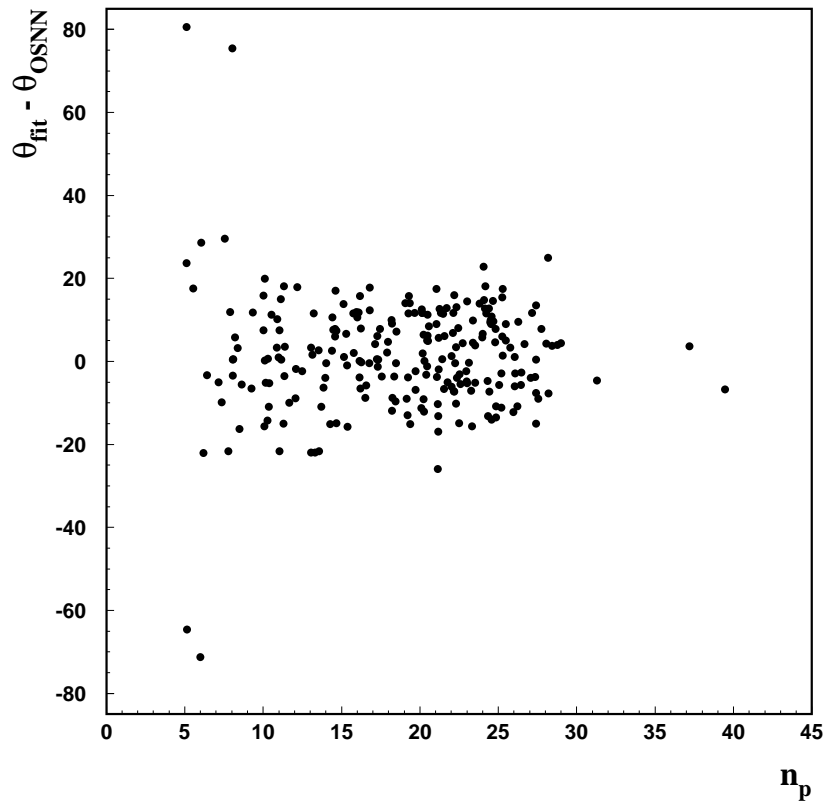


Figure 4: The difference between the muon direction as determined by the highest output from the OSNN, θ_{OSNN} , and the result of a straight line fit, θ_{fit} , as a function of the number of pixels activated in the input layer n_p .

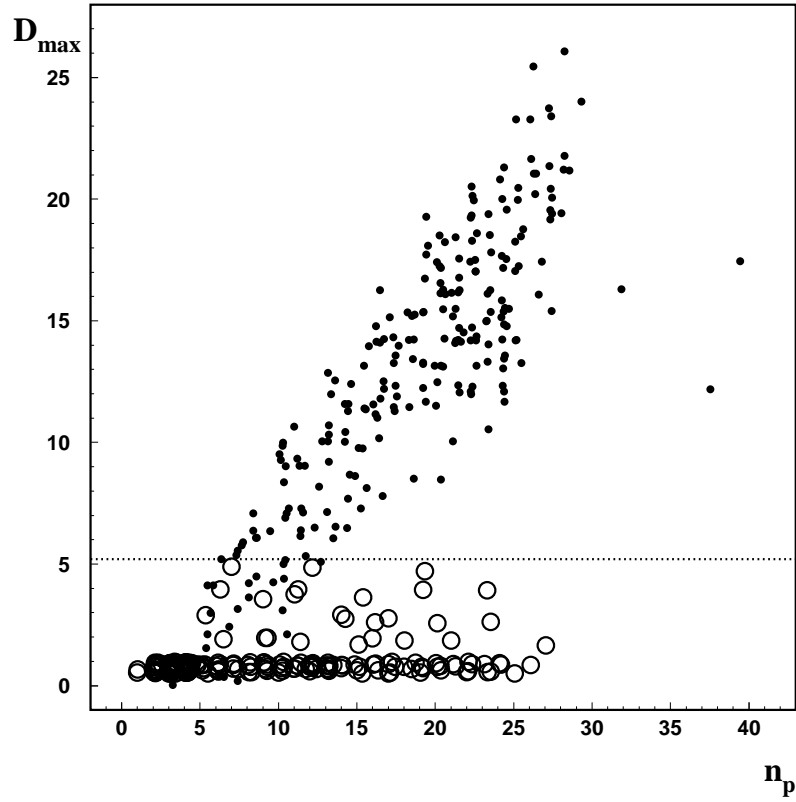


Figure 5: Correlation between the maximum value of D^α , D_{\max} , and the number n_p of input pixels for cosmic muon (dots) and accelerator events (open circles). The dashed line defines a separator such that all events above it correspond to cosmic muons (100% purity). This selection criterion has 92.2% efficiency.

5 The Hough Transform

A well known approach to detection of lines in an image is the application of the Hough transform [7, 8, 9]. This method consists of a preliminary conversion of the Cartesian space into a new parameter space. A line can be parameterized by two values θ and r according to the following expression:

$$r = x \cos \theta - y \sin \theta. \quad (5)$$

A point (x_i, y_i) in the Cartesian plane transforms into a curve in the (r, θ) plane corresponding to all possible lines passing through this point. An intersection point (r_k, θ_k) of two curves in the (r, θ) plane indicates that the two points lie on a straight line in the Cartesian plane. Thus, several points lying on a straight line in the Cartesian plane produce an high-order intersection point in the (r, θ) plane.

When the straight line is probed with a finite resolution, like in the case we are studying, one has to resort to a coarse graining of the parameter plane and to search for an *intersection region* rather than an intersection point. To each pixel activated in the input layer of our Cartesian lattice we assign coordinates corresponding to the geometrical center of the pixel (x_i, y_i) that determine a curve as given by equation 5. We discretize the (r, θ) space into bins and count the number of curves that pass through them. The size of the bins is optimized to give the best sensitivity to linear patterns.

For each event, cosmic muon and accelerator, we determine the maximum number of lines that cross one bin – N_{\max} . In figure 6 we present the distribution of N_{\max} as a function of n_p for the two classes of events. As expected, N_{\max} is on the average larger for cosmic muons than for accelerator events. However we observe that the overlap between the two classes of events is very large. In fact for a 100% purity of the cosmic-muon sample the efficiency is as low as 47%. This can be achieved by the linear separator indicated on the figure. Obviously this result is much worse than the OSNN- D method described in the previous Section. Note that in figure 5 the accelerator events were characterized by low D values which did not rise as function of n_p , thus allowing for a good separation. Regrettably, this is not the case for N_{\max} vs n_p .

There are two reasons why the Hough transform performs poorly in this context. The first one is that our linear patterns are thick. In order to observe a definite enhancement in the (r, θ) space we have to allow for many (x_i, y_i) lying on a thin line to contribute. We thus loose sensitivity to thick linear patterns which include some natural jitter on the square lattice. The other reason is that the Hough transform is not directly sensitive to the inactive pixels lying on a straight line. This is to say that three non consecutive pixels lying on a straight line will look the same as three consecutive ones in the (r, θ) space. Both these features are properly handled by the OSNN.

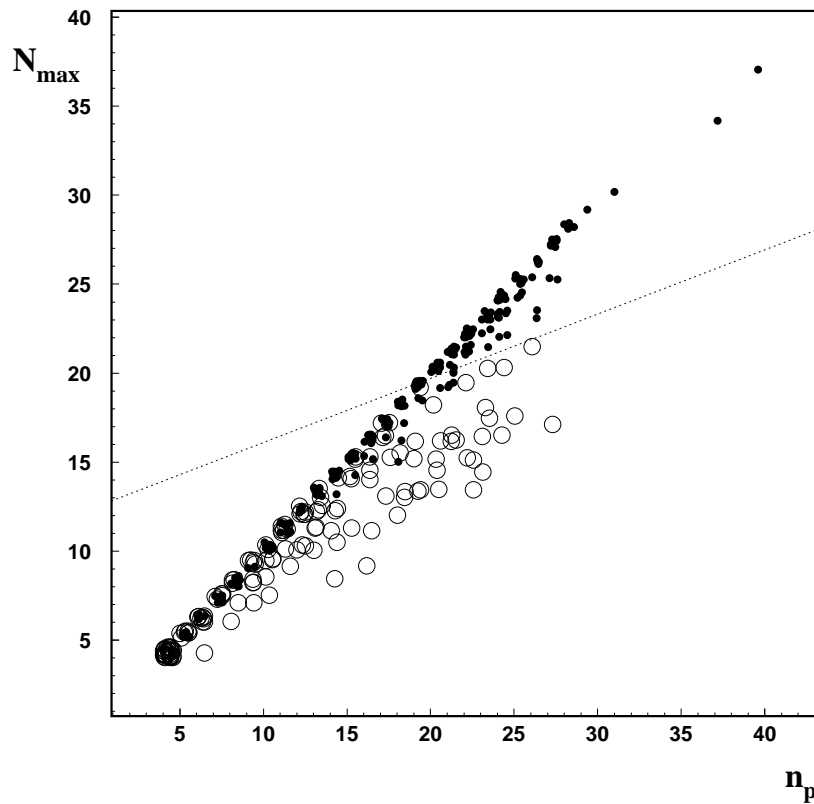


Figure 6: Correlation between the Hough value of N_{\max} , and the number n_p of input pixels for cosmic muon (dots) and accelerator events (open circles). The dashed line defines a separator such that all events above it correspond to cosmic muons (100% purity). This selection criterion has only 47% efficiency.

6 OSNN Selection Procedures

In an effort to improve further the performance of the OSNN we have looked into the possibility of using more information from the fourth layer. In particular, taking into account the angular resolution of the orientation filters we selected the three leading D^α and looked at the sum of the three terms. For a 100% purity the efficiency improved slightly and became 93.7%.

If instead of applying a simple cut we use a neural network to search for the best classification of events with the OSNN outputs, we obtain still better results. The auxiliary network has 6 inputs, one hidden layer with 5 nodes and one output unit. The input consists of a set of five consecutive D^α centered around D_{\max} and the total number of activated input pixels, n_p . The cosmic muons are assigned an output value $s = 1$ and the accelerator events $s = 0$. The net is trained on our sample with error back-propagation. This results in an improved separation of cosmic muon events from the rest. In particular for $s \geq 0.6$ no accelerator events are found and the muons are selected with an efficiency of 96%. This selection procedure will be denoted as OSNN- S .

In order to compare the separation capability of OSNN- D and OSNN- S we present in figure 7 the distribution of the cosmic-muon and accelerator events of the training sample in each of the respective variables, D_{\max} and s . For the presentation D_{\max} has been rescaled by the maximum value it achieved on the training sample. The OSNN- S is slightly better than OSNN- D in that there is a better separation of the two classes of events.

7 Performance of OSNN- S on a Test Sample

Defining our final procedure as the OSNN with the auxiliary neural network, OSNN- S , we apply it to a sample of 39,244 data events which passed the standard physics cuts [5]. The distribution of the neural network output s is presented in figure 8. It looks very different from the one obtained with the training sample. Whereas the former consisted of approximately 500 events distributed equally among accelerator events and cosmic muons, this one contains mostly accelerator events, with less than 1% of muons. This proportion is characteristic of physics samples. The distribution is approximately exponential with a long tail towards larger values of s and a small enhancement at $s = 1$.

We first perform a visual scan of all 138 events with $s \geq 0.1$. The cut is motivated by the performance on the training sample. The scan is based on the full information from the detector. The results are shown in figure 8, where the cosmic-muon events are represented by the shaded area. We find 56 cosmic-muon events and 82 accelerator events. As expected the muons populate mainly the region of large s values.

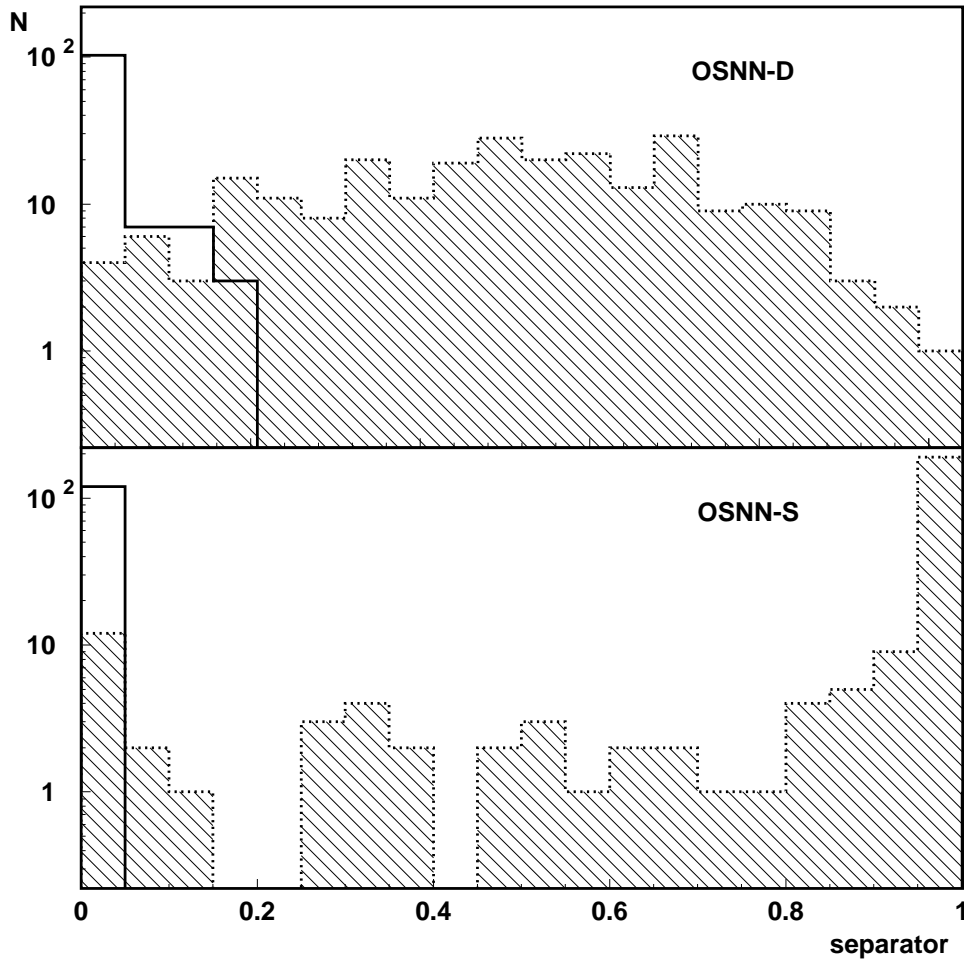


Figure 7: Comparison of two OSNN separation methods: OSNN- D , based on the D_{\max} criterion, and OSNN- S , based on the auxiliary neural network. For the sake of comparison the separator for OSNN- D has been defined as D_{\max} rescaled by the maximum value achieved for the training sample. For OSNN- S the separator is defined as the output of the auxiliary neural net s . Accelerator events are depicted by the solid line, while muons are represented by the shaded area.

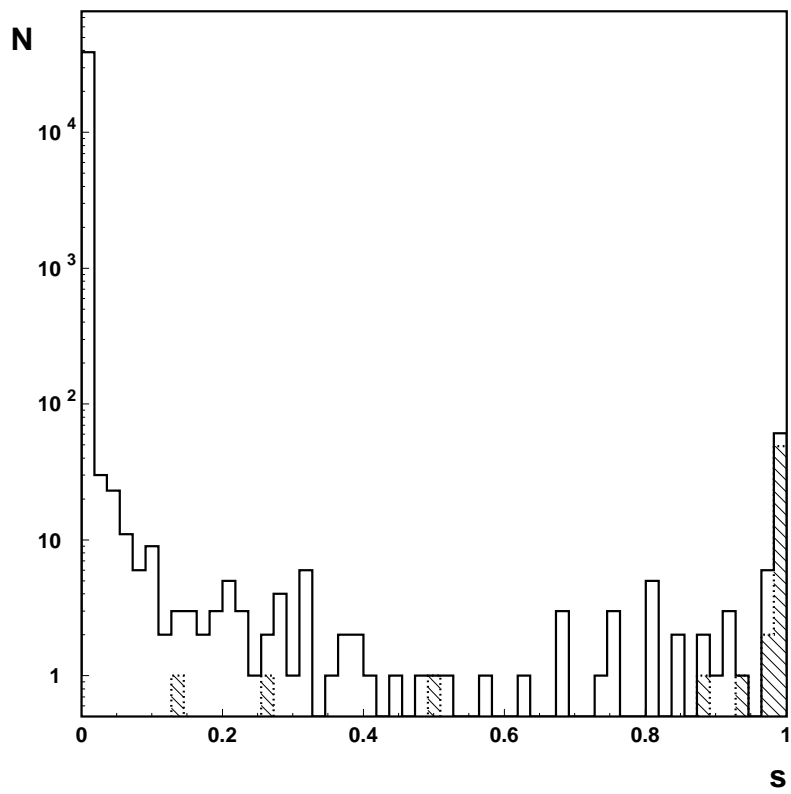


Figure 8: Distribution of the auxiliary neural network output s obtained with the OSNN- S selector for the test sample. Cosmic muons are represented by the shaded areas.

Having now the benefit of a huge sample we see that the tail of the accelerator events spreads to much larger values of s than in the training sample. It should be emphasized that this test sample is judged by different criteria from those used on the training sample. Here cosmic muons or accelerator events are identified as such by the information which is available from the whole detector, which is much more than the two dimensional projection of its rear part which is used as an input to the OSNN. A visual scan based solely on the two-dimensional representation of the rear part of the ZEUS calorimeter reveals that 51 out of the 82 accelerator events look like short cosmic-muon events.

For the sake of completeness we have also looked into the sample of events with $s < 0.1$. Using the full information from the detector supplemented by a visual scan of events likely to be cosmic muons we find 15 cosmic-muon events. Most of these events would be classified as accelerator events based on the information that is available to the OSNN.

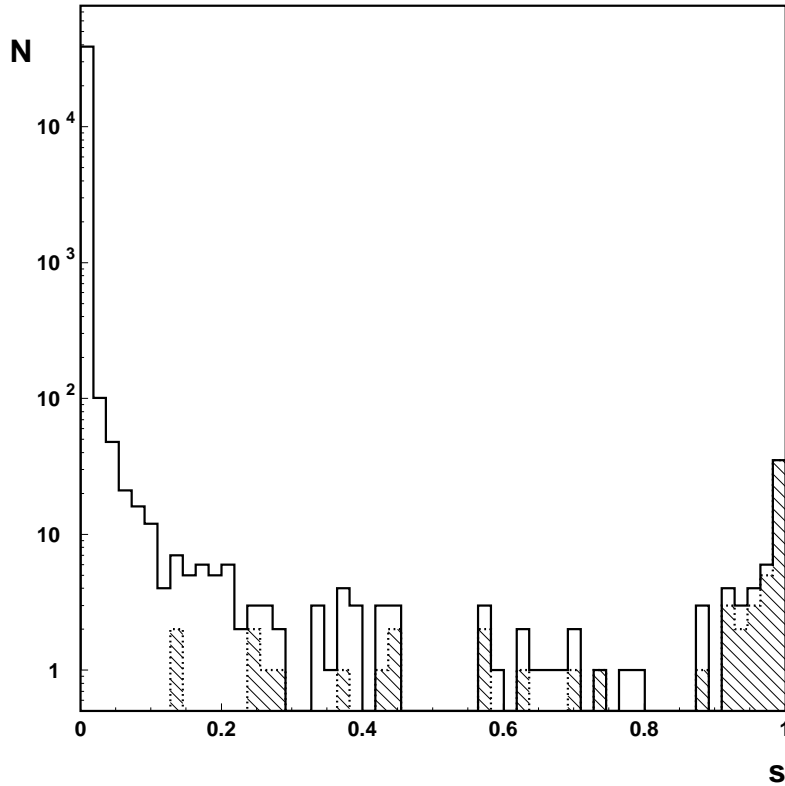


Figure 9: Distribution of the auxiliary neural network output s obtained after retraining the network on the test sample. Cosmic muons are represented by the shaded areas.

Keeping our basic OSNN structure, we decided to use the new sample of 138 events with $s \geq 0.1$ for retraining the auxiliary network. This was then applied to the whole sample of 39,244 events, resulting in a more pronounced bimodal distribution, as shown in figure 9. This suggests using $s = 0.5$ as a separation point. We find then 54 out of the 71 muons of the total sample. This domain is still contaminated by 15 accelerator events, 13 of which resemble muons on the input layer of the OSNN. For comparison, before retraining 37 accelerator events were found for $s \geq 0.5$. The retraining procedure shifted a few of the high- s accelerator events to lower s values, thus leading to a better separation between cosmic-muon and accelerator events.

To check the stability of our procedure we apply the retrained OSNN- S to a new test set. The result is displayed in figure 10. This set contains 40,886 events, and its s distribution is similar to the retraining set of figure 9. We repeat the scanning procedure described above and obtain very similar results. The cosmic muons found with the full detector information for events with $s \geq 0.1$ are displayed by the shaded area. For $s \geq 0.1$ we find 27 cosmic-muon events and 51 accelerator events, out of which 16 look like cosmic-muons at the input of the OSNN. For $s \geq 0.5$ we find 10 accelerator events contaminating a sample of 25 muons, however 8 out of the 10 events look like cosmic-muons at the input of the OSNN. Interestingly enough, a visual scan of 122 events below $s = 0.1$, selected as possible muon candidates because only the rear part of the detector was activated, revealed no further muons.

We learn therefore that our method is stable and reproducible. Its remaining imperfection is due to the fact that the information that is fed into the OSNN comes from only one part of the detector. Even with all its limitations it reduces the problem of rejecting cosmic-muon events down to scanning a fraction of a percent of all the events. We conclude that we have achieved the goal that we set for ourselves, that of replacing a laborious visual scan by a computer algorithm with similar reliability.

8 Summary

We have presented an algorithm for identifying linear patterns on a two-dimensional lattice based on the concept of an orientation selective cell, a concept borrowed from neurobiology of vision. Constructing a multi-layered neural network with fixed architecture which implements orientation selectivity, we define output elements corresponding to different orientations, which allow us to make a selection decision. The algorithm takes into account the granularity of the lattice as well as the presence of noise and inefficiencies.

It has been applied successfully to a sample of events collected with the ZEUS detector at HERA. We find a high efficiency and purity for identifying

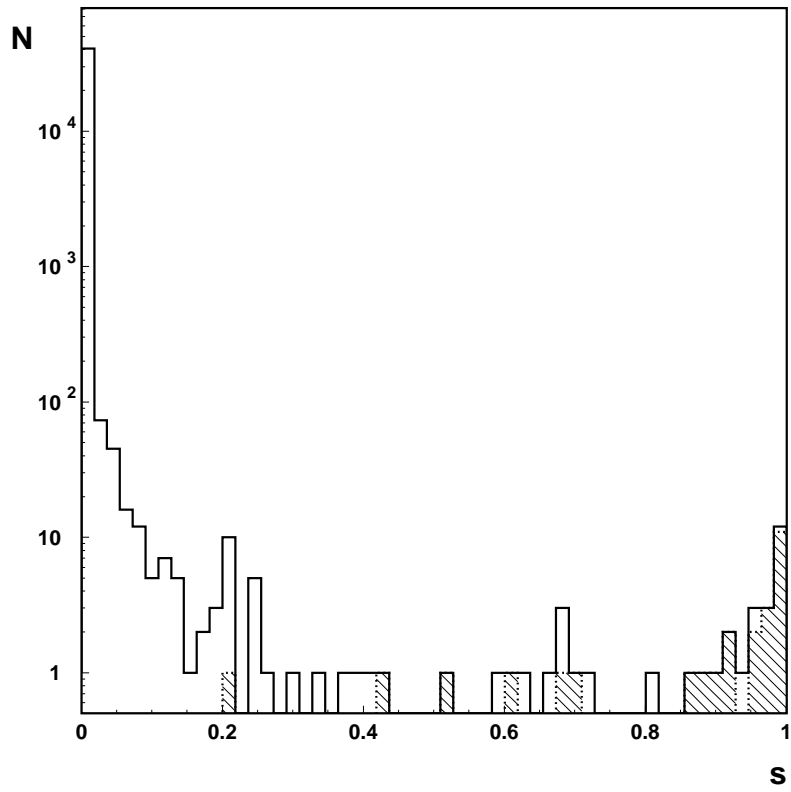


Figure 10: Distribution of the auxiliary neural network output s obtained with the retrained OSNN- S selector for the new test sample. Cosmic muons are represented by the shaded areas.

cosmic muon events which leave a linear pattern of signals in the rear part of the ZEUS calorimeter.

Since we use a fixed architecture, the complexity of our OSNN is not very high. It has, though, a relatively large number of elements, which increases proportionally to the number of pixels and the number of orientations which is appropriate for a given analysis. Such an architecture is suitable for hardware implementation, in which case it can provide for very fast parallel computation.

Acknowledgements

We are indebted to the ZEUS Collaboration for allowing us to use the sample of data for this analysis. This work was partly supported by the Israel Science Foundation.

References

- [1] D. Marr, "Vision". Freeman, San Francisco, 1982.
- [2] T. Poggio and S. Edelman, Nature 343 (1990) 263.
- [3] D. H. Hubel and T. N. Wiesel, J. Physiol. 195 (1968) 215.
- [4] ZEUS Collab., The ZEUS Detector, Status Report 1993, DESY 1993; M. Derrick et al., Phys. Lett. B 293 (1992) 465.
- [5] ZEUS collab., M. Derrick et al., Phys. Lett. B 316 (1993) 412; DESY 95-193 accepted for publication in Z. Phys..
- [6] ZEUS Calorimeter Group, A. Andresen et al., Nucl. Inst. Meth. A 309 (1991) 101.
- [7] P. V. Hough, "Methods and means to recognize complex patterns", U.S. patent 3.069.654.
- [8] D. H. Ballard, Pattern Recognition 3 (1981) 11.
- [9] R. O. Duda and P. E. Hart, Commun. ACM. 15 (1972) 1.